

Physics-inspired spatiotemporal-graph AI ensemble for gravitational wave detection

Minyang Tian^{1,2,3}, E.A. Huerta^{1,2,4,*}, and Huihuo Zheng⁵

¹Data Science and Learning Division, Argonne National Laboratory, Lemont, Illinois 60439, USA

²Department of Physics, University of Illinois at Urbana-Champaign, Urbana, Illinois 61801, USA

³NCSA, University of Illinois at Urbana-Champaign, Urbana, Illinois 61801, USA

⁴Department of Computer Science, The University of Chicago, Chicago, Illinois 60637, USA

⁵Leadership Computing Facility, Argonne National Laboratory, Lemont, Illinois 60439, USA

*Corresponding author: elihu@anl.gov

ABSTRACT

We introduce a novel method for gravitational wave detection that combines: 1) hybrid dilated convolution neural networks to accurately model both short- and long-range temporal sequential information of gravitational wave signals; and 2) graph neural networks to capture spatial correlations among gravitational wave observatories to consistently describe and identify the presence of a signal in a detector network. These spatiotemporal-graph AI models are tested for signal detection of gravitational waves emitted by quasi-circular, non-spinning and quasi-circular, spinning, non-precessing binary black hole mergers. For the latter case, we needed a dataset of 1.2 million modeled waveforms to densely sample this signal manifold. Thus, we reduced time-to-solution by training several AI models in the Polaris supercomputer at the Argonne Leadership Supercomputing Facility within 1.7 hours by distributing the training over 256 NVIDIA A100 GPUs, achieving optimal classification performance. This approach also exhibits strong scaling up to 512 NVIDIA A100 GPUs. We then created ensembles of AI models to process data from a three detector network, namely, the advanced LIGO Hanford and Livingston detectors, and the advanced Virgo detector. An ensemble of 2 AI models achieves state-of-the-art performance for signal detection, and reports seven misclassifications per decade of searched data, whereas an ensemble of 4 AI models achieves optimal performance for signal detection with two misclassifications for every decade of searched data. Finally, when we distributed AI inference over 128 GPUs in the Polaris supercomputer and 128 nodes in the Theta supercomputer, our AI ensemble is capable of processing a decade of gravitational wave data from a three detector network within 3.5 hours, i.e., 2.5×10^4 X faster than real-time. This work underscores the importance of combining advances in AI and supercomputing to address grand challenges in big data physics experiments.

Introduction

The development of AI methodologies for gravitational wave astrophysics is a booming enterprise. Since 2017¹, there has been a rapid development of AI methods and approaches to create, test and deploy production scale tools for gravitational wave detection. The first class of AI models for gravitational wave detection were designed to describe 2D gravitational wave signal manifolds, comprising the masses, (m_1, m_2) , of non-spinning, quasi-circular binary black hole mergers, and which were capable of detecting true gravitational wave signals with a false positive rate of one misclassification for every 100 seconds of searched data¹⁻³. The development of these AI models required training datasets with a few tens of thousands of modeled signals, and a couple of inexpensive GPUs to complete the training within a few hours. These findings sparked the interest of the gravitational wave community, leading to the organic creation of a vibrant, international community of researchers who are harnessing advances in AI and computing to address timely and pressing challenges in gravitational wave astrophysics⁴⁻¹⁸. These seminal ideas have been applied for signal detection¹⁹⁻²¹ and forecasting²²⁻²⁴ of binary neutron stars, and for the detection and forecasting of neutron star-black hole systems^{22,25}. Comprehensive reviews of this active area of research may be found in Refs.²⁶⁻²⁹.

Promoting these disruptive ideas into production scale frameworks for gravitational wave discovery requires innovation at the interface of AI and supercomputing³⁰. This is because AI models that describe compact binary systems that may be detectable by ground-based interferometric detectors span a high dimensional signal manifold. Assuming astrophysical compact binary sources that spiral into each other following a series of quasi-circular orbits, and whose individual components are spinning and non-precessing, may be described in terms of four parameters, (m_1, m_2, s_1^z, s_2^z) . This 4D signal manifold needs to be smartly and densely sampled to train AI models so as to capture the physics of these gravitational wave sources. This then translates into training datasets that have tens of millions of modeled waveforms, i.e., Terabyte size datasets. Therefore, in order to reduce time-to-solution, it is critical to use distributed training algorithms that optimally utilize between hundreds to

thousands of GPUs in supercomputing platforms. Furthermore, these methodologies enable the design of AI surrogates that incorporate physics and math principles in their architecture, training and optimization. In parallel to these development, it is essential to create new methods to improve the sensitivity and performance of state-of-the-art AI models.

Recent accomplishments at the interface of physics inspired AI and supercomputing include the design of physics inspired AI architectures, training and optimization schemes that leverage thousands of GPUs^{31,32}. These AI surrogates have been used to process from seconds- to years-long datasets of gravitational wave data to demonstrate that AI can be used to search for and find gravitational wave signals with an average false positive rate of one misclassification for every month of searched data^{33,34}. It has also been demonstrated that when these AI surrogates are optimized for accelerated inference with NVIDIA TensorRT, and the inference is distributed over the entire [ThetaGPU supercomputer](#) at the Argonne Leadership Computing Facility, consisting of 160 NVIDIA A100 Tensor Core GPUs, gravitational wave data can be processed over 52,000X faster than real-time assuming a two detector network comprising the twin advanced LIGO detectors³⁵.

Since AI advances in gravitational wave astrophysics exhibit great promise, in this article we contribute to this line of research by designing AI architectures, training and optimization methods that incorporate physics and geometrical principles involved in the detection of gravitational waves. In practice, we have designed neural networks that capture both short- and long-range temporal dependencies of gravitational wave signals with hybrid dilated convolution networks. We also incorporate geometrical and spatial considerations of signal detection in terms of the location of gravitational wave detectors through graph neural networks. We show that this approach improves the sensitivity of AI ensembles for signal detection, while also reducing the number of false positives to 7 misclassification for every decade of searched data when using an ensemble of two AI models, and to 2 misclassification for every decade of searched data when using an ensemble of 4 AI models. This is the first time AI methods achieve this level of accuracy over decade-long datasets.

We showcase this approach in the context of a network of three ground-based gravitational wave detectors encompassing the twin advanced LIGO and advanced Virgo detectors. We present results for two types of astrophysical populations, namely, quasi-circular, non-spinning binary black hole mergers, as well as quasi-circular, spinning, non-precessing binary black hole mergers. We showcase how to reduce time-to-solution by using distributed training on the [Polaris supercomputer](#) at the Argonne Leadership Supercomputing Facility, in which we used 256 NVIDIA A100 GPUs to train AI models within 1.7 hours, while also ensuring optimal classification performance. We also demonstrate that our approach presents strong scaling up to 512 NVIDIA A100 GPUs. We also used 128 NVIDIA A100 GPUs in Polaris and 128 nodes in the Theta supercomputer to process a decade's worth of simulated advanced gravitational wave data from a three detector networks within 3.5 hours, i.e., 25,000X faster than real-time.

Results

We present two types of results to quantify the ability of our AI models to search for and find gravitational waves in a decade-long gravitational wave dataset in which we consider a three detector network comprising the twin advanced LIGO detectors and the advanced Virgo detector. The first set of results describes an astrophysical population of quasi-circular, non-spinning binary black hole mergers. The second set of results extends the previous analysis for a population of quasi-circular, spinning, non-precessing binary black hole mergers.

In the Methods section we describe in detail the datasets and modeled waveforms used for these studies, and approaches we have developed to train AI models at scale, and to enable hyper-efficient AI inference of large scale gravitational wave datasets in leadership class supercomputers.

Quasi-circular, non-spinning binary black hole mergers

Here we consider a binary black hole population whose individual masses, (m_1, m_2) , span the range $m_{\{1,2\}} \in [3M_{\odot}, 50M_{\odot}]$. To instill the physics of these astrophysical sources into our AI surrogates, we have produced datasets of modeled waveforms using the `IMRPhenomXPHM` model³⁶. These waveforms are then curated to simulate a variety of astrophysically motivated scenarios, i.e., we consider a broad range of signal-to-noise ratios (SNR), sky locations, mass combinations, etc. This approach ensures that AI models are capable of correctly identifying gravitational waves that may be produced in a wide variety of astrophysical scenarios. Once our AI models are fully trained, we test them with new datasets that have not seen by these AI models during training. These new datasets contain either pure noise, or noise plus injected signals that simulate detection scenarios.

Figure 1 presents two types of metrics we used to quantify the performance of our AI models for signal detection, i.e., the Receiver Operating Characteristic (ROC) curve and the Precision-Recall (PR) curve. Therein we present results for three cases, in which we construct ensembles that include, 2 AI models (top row), 3 AI models (center row), and 4 AI models (bottom row), respectively. These results were produced assuming that the AI ensembles processed a decade-long dataset that describes a three detector network that comprises the advanced LIGO and advanced Virgo detectors. We injected 300,000 modeled waveforms in this test set, and quantified the ability of AI ensembles to correctly identify injected signals, and discard other noise anomalies. Key results we extract from these studies include the following:

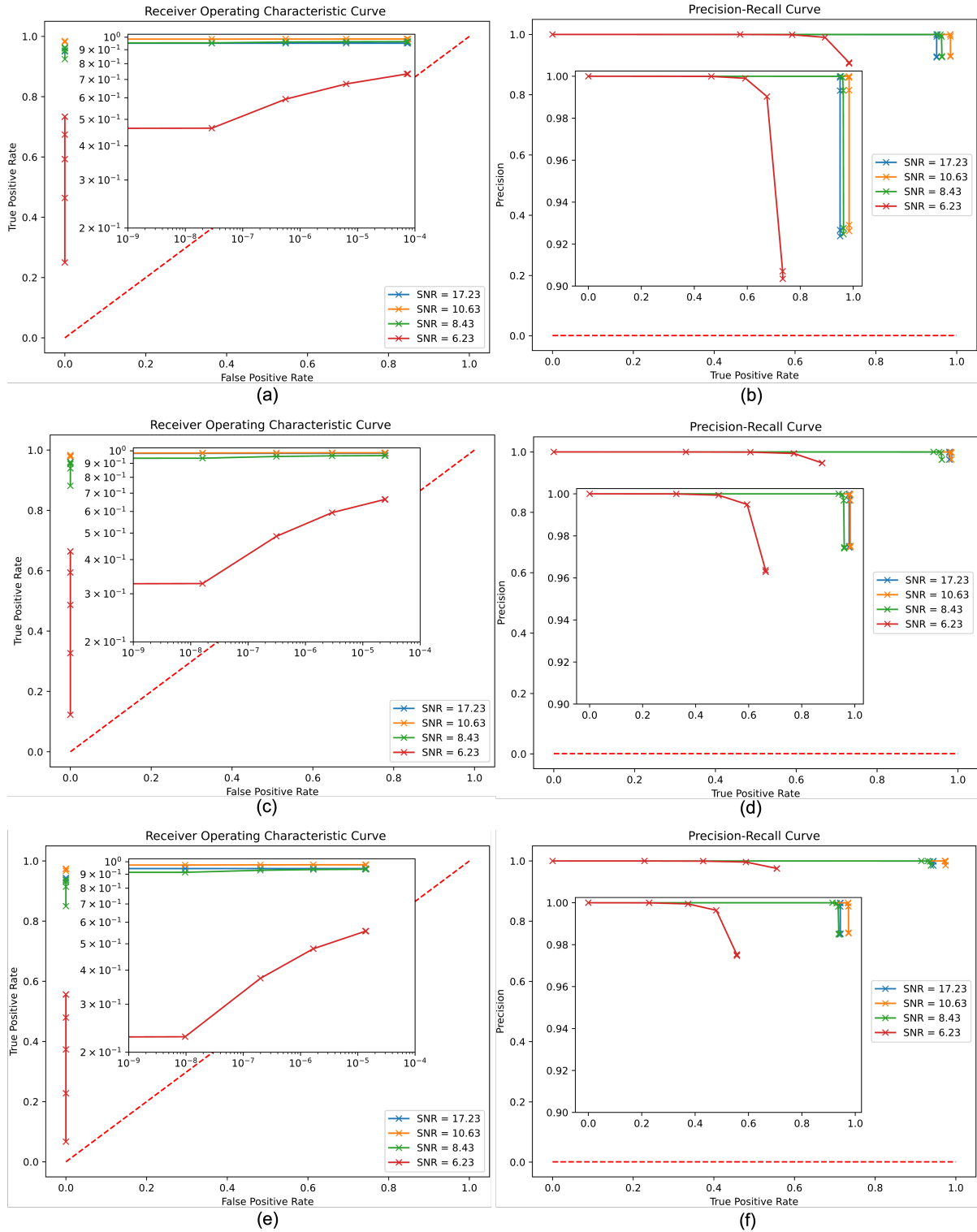


Figure 1. Classification performance of AI ensembles to detect quasi-circular, nonspinning black hole mergers. Classification performance in terms of the Receiver Operating Characteristic (ROC) curve, and the Precision-Recall (PR) curve for ensembles that include 2 AI models (top row), 3 AI models (center row), and 4 AI models (bottom row). These results were produced using a decade-long gravitational wave test set, for the advanced LIGO and advanced Virgo three detector network, in which we injected 300,000 modeled binary black hole waveforms that cover a broad SNR range.

# of models	FP	ROC AUC		PR AUC	
		SNR ₁	SNR ₂	SNR ₁	SNR ₂
2	9	0.9817	0.9923	0.9633	0.9845
3	5	0.9802	0.9918	0.9603	0.9835
4	3	0.9691	0.9873	0.9382	0.9746

Table 1. Classification performance of AI ensembles that include 2, 3 or 4 AI models (left column). Here we consider a population of quasi-circular, nonspinning binary black hole mergers. FP presents the number of false positives reported by the AI ensembles upon processing a decade-long gravitational wave test set that describes a three detector network comprising the advanced LIGO and advanced Virgo detectors, and in which we injected 300,000 modeled waveforms that cover a broad range of signal-to-noise ratios (SNRs). We also present additional figures of merit, namely, the Area Under the Curve (AUC) for the Receiver Operating Characteristic (ROC) curve, and the Precision-Recall (PR) curve for two SNR values that represent the bulk of events detected thus far by advanced LIGO and advanced Virgo, i.e., SNR₁ = 8.4, and SNR₂ = 10.6—see also Figure 1.

- Figure 1 shows that AI’s precision to detect gravitational waves improves as we increase the number of AI models in the ensemble (right column). At the same time, there is a marginal reduction in the true positive rate, in particular for low SNR signals (both left and right column).
- We provide key figures of merit in Table 1. Therein we show that a 2 AI model ensemble reports 9 false positives per decade, a 3 AI model ensemble reports 5 false positives per decade, while a 4 AI model ensemble produces 3 misclassifications per decade of searched data. We also present the Area Under the Curve (AUC) for the ROC and PR curves for gravitational wave signals in our 300,000 test set with SNR₁ = 8.4 and SNR₂ = 10.6. We selected these SNR values since they provide a fair representation of the bulk of events reported in the Gravitational Wave Open Science Center³⁷. These results show that as we consider larger AI ensembles there is marginal decrease in the ROC AUC and PR AUC for low SNR signals, while signals with SNR₂ = 10.6 have a negligible change.

This work significantly outperforms recent results in the literature^{34,35}, in which AI models were used to process a 5 year-long dataset. Here we significantly improve the classification performance of those AI models, both in terms of improving the true positive rate for signals across SNRs, and with a very significant improvement for low and moderate SNR signals (compare these findings to those in Figure 4 in³⁴). We also reduce the number of misclassifications from 1 per month to 3 per decade. This is the first time AI reaches this level of accuracy to correctly tell apart gravitational waves from other noise anomalies. Given the quality of these results, we decided to extend this analysis for a population of quasi-circular, spinning, non-precessing binary black hole mergers. We do this because this 4D signal manifold contains much more astrophysical content given the richer morphology and time-evolution of gravitational wave signals, and thus we expect that AI models trained with these datasets will be able to enhance the capabilities of AI for signal detection.

Quasi-circular, spinning, non-precessing binary black hole mergers

Here we extend the previous analysis, considering a population of quasi-circular, spinning, non-precessing binary black hole mergers. This signal manifold is described by 4 parameters, namely, (m_1, m_2, s_1^z, s_2^z) . As before, the binary components of these systems span the range $m_{\{1,2\}} \in [3M_\odot, 50M_\odot]$, while their individual spins cover the range $s_{\{1,2\}}^z \in [-0.9, 0.9]$. The depth of this parameter space requires Terabyte-size datasets of modeled waveforms needed to adequately capture the physics of these systems. However, this is important to ensure that AI models are trained to identify waveforms that describe astrophysical black hole mergers in which black holes have non-negligible spin.

As before, once our AI surrogates are fully trained, we selected the top performers, and create ensembles to process synthetic data from the advanced LIGO and advanced Virgo detectors. Results for datasets that span ten years of data are presented in Figure 2.

To dissect these results, let us first compare Figure 2 and Figure 1. We notice that AI ensembles for quasi-circular, spinning, non-precessing binary black hole mergers (AISBH) are better at detecting gravitational waves than AI ensembles for quasi-circular, nonspinning binary black hole mergers (AIBH). We draw this conclusion because

- The precision of AISBH is superior than that of AIBH irrespective of the size of the AI ensemble (compare right column of each Figure).
- The true positive rate of AISBH decreases only marginally, in particular for low SNR signals, while its precision increases as we use larger AI ensembles.
- As shown in Table 2, the number of false positives over a decade of searched data is 7, 3 and 2 as we consider AI ensembles with 2, 3 and 4 AI models.
- According to Table 2, the ROC AUC and PR AUC changes marginally as we increase the size of the AI ensemble.

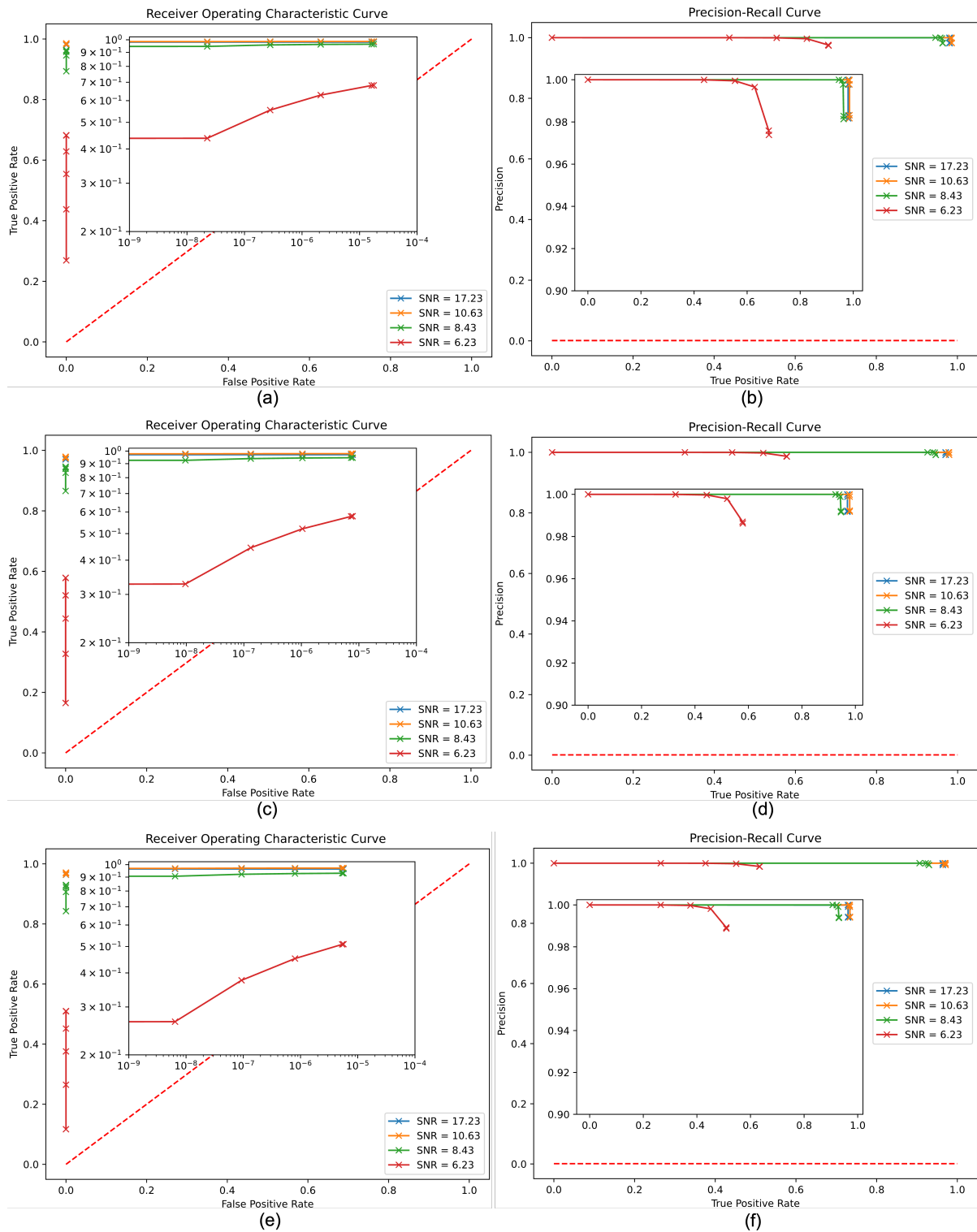


Figure 2. Classification performance of AI ensembles to detect quasi-circular, spinning, non-precessing black hole mergers. As Figure 1, but now for a population of quasi-circular, spinning, non-precessing binary black hole mergers.

# of models	FP	ROC AUC		PR AUC	
		SNR ₁	SNR ₂	SNR ₁	SNR ₂
2	7	0.9818	0.9929	0.9636	0.9857
3	3	0.9730	0.9894	0.9460	0.9789
4	2	0.9649	0.9855	0.9297	0.9710

Table 2. As Table 1, but now for AI ensembles that describe a population of quasi-circular, spinning, non-precessing binary black hole mergers.

In brief, AI ensembles trained with modeled waveforms that describe quasi-circular, spinning, non-precessing binary black hole mergers provide optimal results. As we argued before, this is because these AI models are exposed to signals with more complex morphology and time-evolution, and thus are better equipped at telling apart true signals from other noise anomalies. Again, if compare these results to those presented in Refs.^{34,35}, we notice that the AI models and computational methods we introduce in this paper significantly improve the capabilities of AI for signal detection by enhancing its precision and accuracy, and by significantly reducing the number of false positives over long datasets.

These results provide the necessary information for researchers to develop detection strategies that meet their needs.

Methods

Here we describe in detail the datasets, AI architectures, training and optimization schemes used to create our AI models.

Datasets We used the `IMRPhenomXPHM` waveform model³⁶ to create datasets of modeled waveforms, sampled at 4096 Hz, that describe an astrophysical population of binary black holes that spiral into each other following a series of quasi-circular orbits. Their binary components span the masses $m_{\{1,2\}} \in [3M_{\odot}, 50M_{\odot}]$, and individual spins $s_{\{1,2\}} \in [-0.9, 0.9]$. We generated 1.8 million waveforms by uniformly sampling this (m_1, m_2, s_1^z, s_2^z) parameter space. Furthermore, we incorporated information about the sky location and detector location into the modeled waveforms by sampling right ascension and declination, orbital inclination, coalescence phase, and waveform polarization. Right ascension and declination are sampled uniformly on a solid angle of a sphere. The polar angle varies from $\pi/2$ (north pole) to $-\pi/2$ (south pole). The orbital inclination is sampled using a $\sin(\text{inclination})$ -distribution. The coalescence phase and waveform polarization are both uniformly sampled covering the range $[0, 2\pi)$. We have densely sampled these parameters to expose our AI surrogates to a broad range of plausible detection scenarios. With this approach, our AI surrogates learn the interplay between these parameters, and the slightly different times at which the merger event (waveform amplitude peak) is recorded by our AI surrogates in their three input data channels, representing the advanced LIGO and advanced Virgo detectors.

Out of the 1.8 million waveforms in our dataset, we have created three independent, non-overlapping datasets. The training set has 1.2 million waveforms, whereas the validation and test sets have 300,000 modeled waveforms each.

Power Spectral Density for advanced LIGO and advanced Virgo To model the sensitivity of advanced LIGO and advanced Virgo detectors, we rely on Power Spectral Density (PSD) curves. Specifically, we use PSD curves from advanced LIGO Sensitivity (190 Mpc) based on the fourth observing run (O4) for the Hanford and Livingston detectors. For advanced Virgo detector, we use PSD data from the fifth observing run (O5), which has a low noise and high range limit target sensitivity³⁸.

Data curation Modeled waveforms were whitened with the aforementioned PSDs. We also produced synthetic noise, and colored it with the PSDs representing each of the detectors. To address the challenge posed by highly imbalanced data in real detection, our dataset uses 70% negative samples (only noise) and 30% positive samples (noise and signals).

For generating negative samples in our model, we randomly select 1s-long segments of pure noise from the generated synthetic noise. These negative samples are labeled as pure 0s. On the other hand, for generating positive samples, we truncate the whitened signal to the 0.5s before the merger and the ringdown part. Thereafter, we linearly mixed whitened waveforms and whitened noise so as to describe a broad range of astrophysical scenarios. The label for positive samples will be set to 1 only for the 0.5s before the merger, while the remaining part will be labeled as 0, since we are mostly interested in the merger portion of the signals where the AI models have the sharpest response.

AI model architecture Our neural network model has two building blocks: the hybrid dilated convolution network (HDCN) block, and the graph neural network (GNN) block. The HDCN block is used to handle long-range temporal dependencies that are crucial for signal prediction, while the GNN block merges prediction embeddings from the three detection channels: LIGO Livingston (L), LIGO Hanford (H), and Virgo (V), while considering their spatial relationship. This block also generates the final prediction with an output layer.

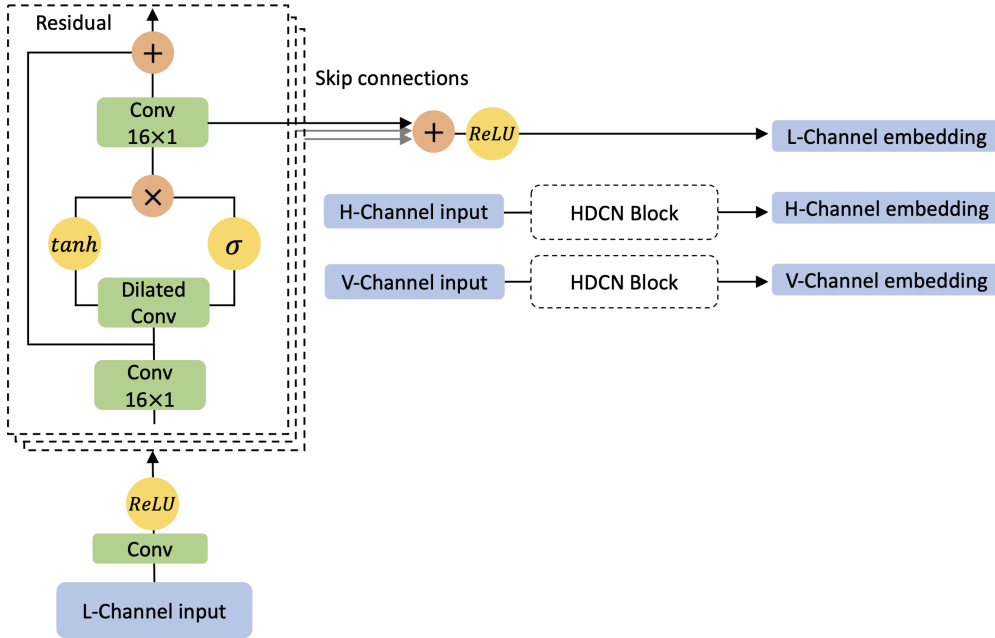


Figure 3. Architecture of hybrid dilated convolution network (HDCN). Each detector input will be processed by an individual HDCN, which consists of the N blocks of pre-processing time-distributed convolution layer, dilated convolution layer, and the post-processing time-distributed convolution layer. N depends on the receptive field desired. Here we use $N=11$ to cover a half second receptive field. Each block has residual structure and skip connection to the output embedding.

Our HDCN block is inspired by WaveNet³⁹, a deep neural network for audio generation tasks, such as human speech or music. It uses dilated causal convolutions to model the temporal dependencies of audio signals, allowing it to generate high-fidelity audio with long-range structure. We believe we can also use it for our high sample rate time-series data, as the dilated convolution layers enable the network to capture larger receptive fields using fewer parameters. Moreover, its block-based structure enables the model to respond to a diverse range of frequency bands.

We present the hybrid dilated convolution structure in Figure 3. It consists of pre-processing and post-processing time-distributed convolution layers and dilated convolution layers. With time-distributed convolution layers, HDCN is able to enlarge the expressiveness of the embedding. By stacking dilated convolution layers with different dilation rates and gated activation unit, HDCN will get an exponential increase in the size of the receptive field with respect to the number of layers. It will be crucial when considering long-range temporal dependencies in our signals. Finally, residual structure and skip connections are used to combine both long-range and short-range dependencies. Every detector strain data will be processed by an i.i.d. HDCN block to output the prediction embeddings since we want to preserve each detector’s own information for the following GNN block.

On the other hand, there are various GNN structures available^{40–44}, and we decided to use the Message Passing Neural Network (MPNN) framework with max pooling as the permutation invariant operator. We believe this can help capture the most important features in the embeddings and discard the less significant ones. Additionally, max pooling can help make the model more robust to small perturbations or noise in the input data by focusing on the strongest features, i.e., on the merger event.

Following the HDCN blocks, we obtain three prediction embeddings from the three detector channels. Since all three embeddings should represent the same true signal generated by the binary black hole merger, we need to combine them to produce the final prediction output. While a naive approach is to concatenate the three channels and pass them through a multi-layer perceptron (MLP)³³, this method is not entirely optimal. If we change the order of the channels, the MLP output will differ even though the channels still represent the same signal. Therefore, we need a more robust approach to combine the embeddings. We use GNN to preserve the permutation invariance between the three detector embeddings and obtain a graph-level embedding as the combined output.

The GNN structure is shown in Figure 4 (a). For each target node, the GNN block applies an Aggregate step and a Combine step. During the Aggregate step, the GNN processes each neighbor embedding using a convolution layer and then uses max pooling to output the aggregated neighbor message, which is permutation invariant. In the Combine step, the GNN concatenates the aggregated neighbor message with the target node embedding and passes the result to another convolution layer to update

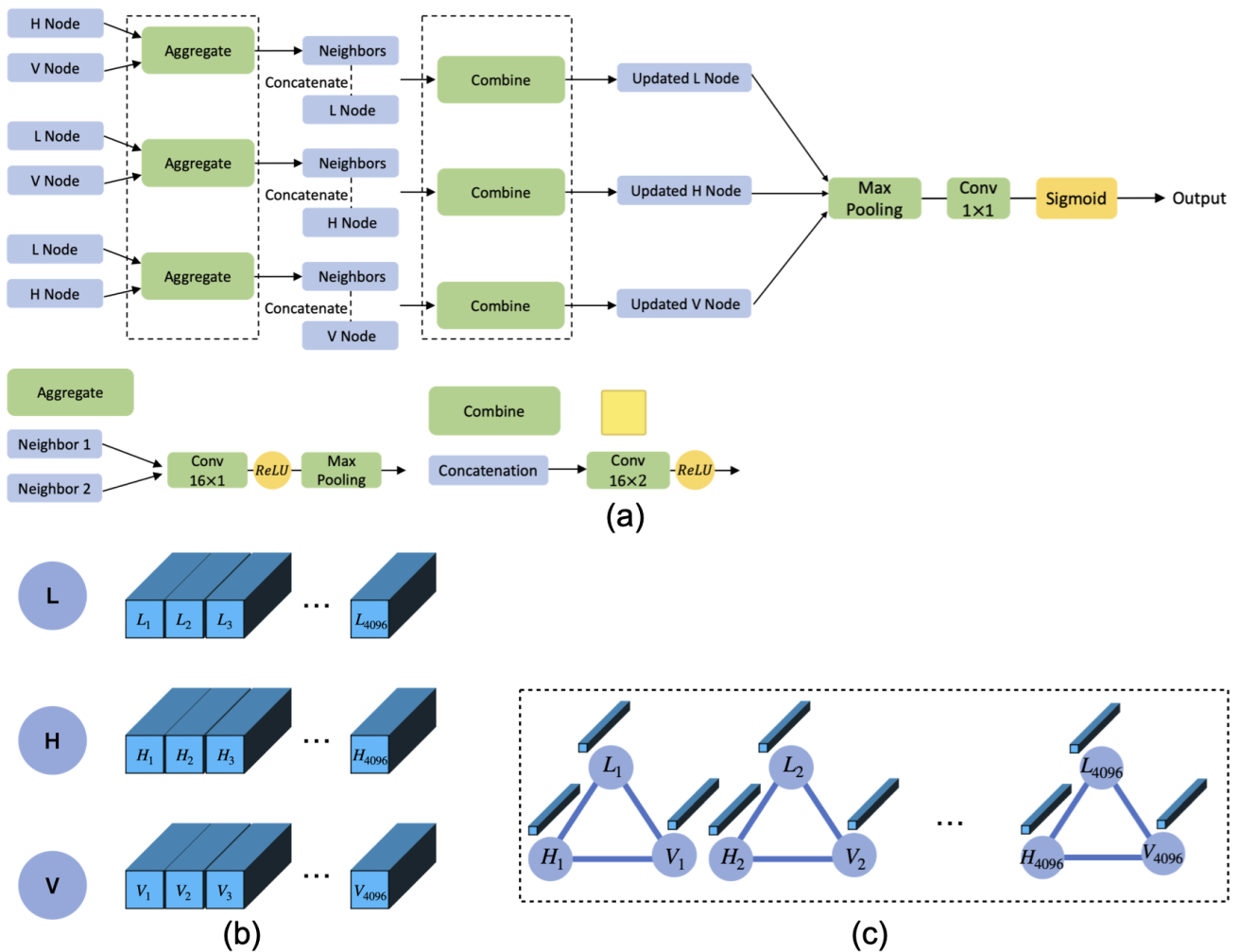


Figure 4. Spatiotemporal-graph AI model structure. (a) Graph neural network (GNN) structure, (b) 3 prediction embeddings given by the hybrid dilated convolution network (HDCN) block, (c) Geometric visualization for prediction embeddings of the three time series produced by the advanced LIGO and advanced Virgo detectors.

the target node embedding. The Aggregate and Combine layer is shared among the 3 nodes. Next, we use max pooling to combine the 3 node embeddings and generate a graph-level embedding. Finally, we apply an MLP with sigmoid activation to the graph-level embedding to generate element-wise predictions.

In the GNN block, we represent each time step as a three-node graph and use the GNN to combine the three embeddings of each time step. Since each time step already encompasses a long receptive field after HDCN, this method is sufficient to generate accurate predictions at each time step. We can easily incorporate multiple-step correlation by increasing the kernel size of the convolution layer accordingly. Then, we apply a general GNN to process the node embeddings, as it captures the relationship between the embeddings, i.e., the locations of the detectors. Since the detector locations remain constant over time, we use the same GNN function for all time steps. This approach has the added benefit of preserving the strong correlation between the embeddings, which is due to their highly overlapping receptive fields. Consequently, we can maintain this correlation in our final time-series prediction output. We can consider each time step as a subgraph in a larger graph, as shown in Figure 4 (c), allowing us to share the aggregation and combination functions across all time steps. In other words, we propose a time-independent GNN to process the time-series embeddings.

Distributed training at scale We conducted scaling tests in the Polaris supercomputer at the Argonne Leadership Computing Facility. In Figure 5 our scaling results. The AI models presented in this article were trained within 1.7 hrs using 256 A100 GPUs. All these models have optimal classification accuracy. We also conducted scaling studies using up to 512 A100 GPUs, in which case the training phase was completed 59 minutes.

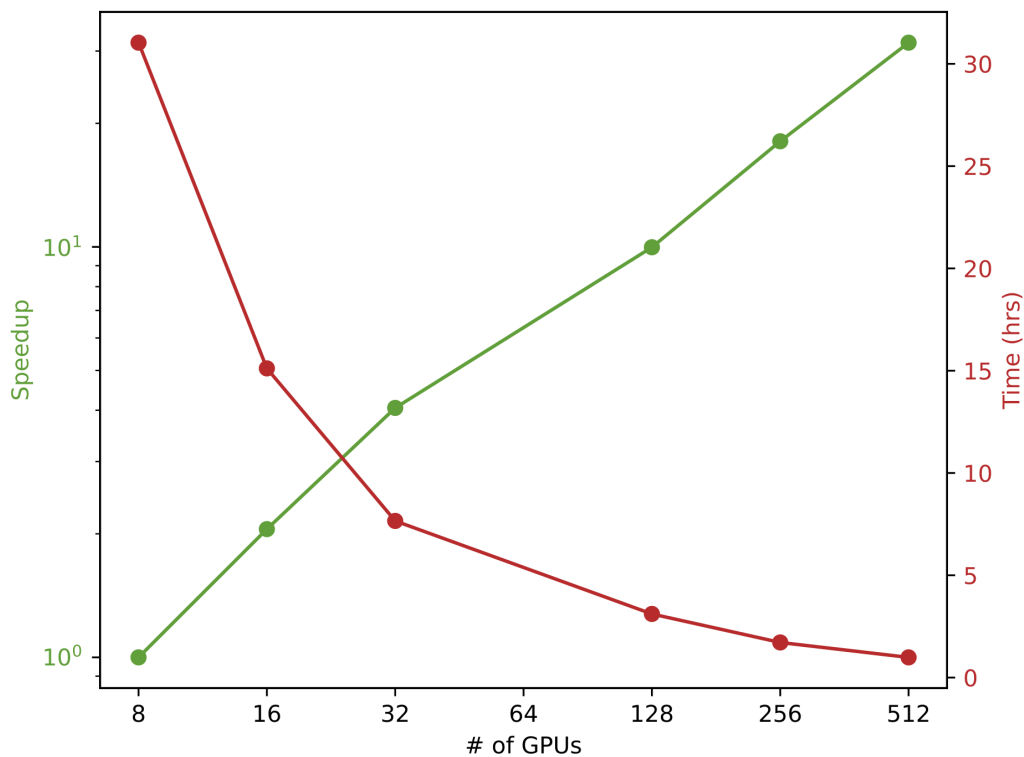


Figure 5. Distributed training in the Polaris supercomputer. We trained AI surrogates within 1.7 hours using 256 A100 NVIDIA GPUs with optimal classification performance. Our optimization method exhibits strong scaling up to 512 GPUs.

AI inference at scale Once we completed the training of multiple AI models with optimal classification performance, we distributed the inference over a decade of simulated gravitational wave data. We first processed these data using our AI ensemble using 128 A100 GPUs in Polaris, and then post-process the AI models’ output using 128 CPU nodes in the Theta supercomputer. The first part is completed within 3.19 hours, while the second is completed in about 0.3 hours. Thus, a decade’s worth of gravitational wave data is processed within 3.5 hours.

Discussion

We have demonstrated how to encapsulate temporal and spatial aspects of gravitational wave detection into a novel spatiotemporal-graph AI model. We have tested this methodology considering 2D and 4D signal manifolds that describe binary black hole mergers. Our findings indicate that AI ensembles can attain optimal signal detection while also reducing the number of false positives to only 2 over a decade of searched data that describes a three detector network. This is the first time AI attains this level of accuracy and sensitivity for gravitational wave detection.

On the algorithm side of things, this work also represents a milestone in the training of AI models that combine hybrid dilated convolution networks and graph neural networks, since we succeeded in training these complex models at scale using up to 256 A100 GPUs with optimal performance, and demonstrated strong scaling using up to 512 A100 GPUs.

In addition to reducing time-to-solution using distributed training, we also distributed AI inference so as to process an entire decade of advanced gravitational wave data within 3.5 hours. In brief, AI provides a natural pathway to accelerate and automate gravitational wave discovery using existing supercomputing resources.

This work will facilitate the development of AI models for signal detection using open source data at the Gravitational Wave Open Science Center to process advanced LIGO and advanced Virgo data at scale. Furthermore, this approach will streamline the development of AI models to search for signals that include higher order waveform modes and spin precession since at this time the training of AI models for 4D signal manifolds may be completed in just under 2 hrs. These studies will be pursued in the future.

Data Availability All data and software used in this article are available upon reasonable request from the authors.

References

1. George, D. & Huerta, E. A. Deep neural networks to enable real-time multimessenger astrophysics. *Phys. Rev. D* **97**, 044039, DOI: [10.1103/PhysRevD.97.044039](https://doi.org/10.1103/PhysRevD.97.044039) (2018). [1701.00008](https://arxiv.org/abs/1701.00008).
2. George, D. & Huerta, E. A. Deep Learning for Real-time Gravitational Wave Detection and Parameter Estimation with LIGO Data. In *NiPS Summer School 2017* (2017). [1711.07966](https://arxiv.org/abs/1711.07966).
3. George, D. & Huerta, E. A. Deep Learning for real-time gravitational wave detection and parameter estimation: Results with Advanced LIGO data. *Phys. Lett. B* **778**, 64–70, DOI: [10.1016/j.physletb.2017.12.053](https://doi.org/10.1016/j.physletb.2017.12.053) (2018). [1711.03121](https://arxiv.org/abs/1711.03121).
4. Gabbard, H., Williams, M., Hayes, F. & Messenger, C. Matching Matched Filtering with Deep Networks for Gravitational-Wave Astronomy. *Phys. Rev. Lett.* **120**, 141103, DOI: [10.1103/PhysRevLett.120.141103](https://doi.org/10.1103/PhysRevLett.120.141103) (2018). [1712.06041](https://arxiv.org/abs/1712.06041).
5. Lin, Y.-C. & Wu, J.-H. P. Detection of gravitational waves using bayesian neural networks. *Phys. Rev. D* **103**, 063034, DOI: [10.1103/PhysRevD.103.063034](https://doi.org/10.1103/PhysRevD.103.063034) (2021).
6. Wang, H., Wu, S., Cao, Z., Liu, X. & Zhu, J.-Y. Gravitational-wave signal recognition of LIGO data by deep learning. *Phys. Rev. D* **101**, 104003, DOI: [10.1103/PhysRevD.101.104003](https://doi.org/10.1103/PhysRevD.101.104003) (2020). [1909.13442](https://arxiv.org/abs/1909.13442).
7. Fan, X., Li, J., Li, X., Zhong, Y. & Cao, J. Applying deep neural networks to the detection and space parameter estimation of compact binary coalescence with a network of gravitational wave detectors. *Sci. China Phys. Mech. Astron.* **62**, 969512, DOI: [10.1007/s11433-018-9321-7](https://doi.org/10.1007/s11433-018-9321-7) (2019). [1811.01380](https://arxiv.org/abs/1811.01380).
8. Li, X.-R., Babu, G., Yu, W.-L. & Fan, X.-L. Some optimizations on detecting gravitational wave using convolutional neural network. *Front. Phys. (Beijing)* **15**, 54501, DOI: [10.1007/s11467-020-0966-4](https://doi.org/10.1007/s11467-020-0966-4) (2020). [1712.00356](https://arxiv.org/abs/1712.00356).
9. Deighan, D. S., Field, S. E., Capano, C. D. & Khanna, G. Genetic-algorithm-optimized neural networks for gravitational wave classification. *Neural Comput. Appl.* **33**, 13859–13883 (2021).
10. Rebei, A. *et al.* Fusing numerical relativity and deep learning to detect higher-order multipole waveforms from eccentric binary black hole mergers. *Phys. Rev. D* **100**, 044025, DOI: [10.1103/PhysRevD.100.044025](https://doi.org/10.1103/PhysRevD.100.044025) (2019). [1807.09787](https://arxiv.org/abs/1807.09787).
11. Beheshtipour, B. & Papa, M. A. Deep learning for clustering of continuous gravitational wave candidates. *Phys. Rev. D* **101**, 064009, DOI: [10.1103/PhysRevD.101.064009](https://doi.org/10.1103/PhysRevD.101.064009) (2020). [2001.03116](https://arxiv.org/abs/2001.03116).
12. Schäfer, M. B. & Nitz, A. H. From one to many: A deep learning coincident gravitational-wave search. *Phys. Rev. D* **105**, 043003, DOI: [10.1103/PhysRevD.105.043003](https://doi.org/10.1103/PhysRevD.105.043003) (2022). [2108.10715](https://arxiv.org/abs/2108.10715).
13. Schäfer, M. B., Zelenka, O., Nitz, A. H., Ohme, F. & Brüggmann, B. Training strategies for deep learning gravitational-wave searches. *Phys. Rev. D* **105**, 043002, DOI: [10.1103/PhysRevD.105.043002](https://doi.org/10.1103/PhysRevD.105.043002) (2022). [2106.03741](https://arxiv.org/abs/2106.03741).
14. Gunny, A. *et al.* Hardware-accelerated inference for real-time gravitational-wave astronomy. *Nat. Astron.* **6**, 529–536, DOI: [10.1038/s41550-022-01651-w](https://doi.org/10.1038/s41550-022-01651-w) (2022). [2108.12430](https://arxiv.org/abs/2108.12430).

15. Schäfer, M. B. *et al.* First machine learning gravitational-wave search mock data challenge. *Phys. Rev. D* **107**, 023021, DOI: [10.1103/PhysRevD.107.023021](https://doi.org/10.1103/PhysRevD.107.023021) (2023). [2209.11146](https://arxiv.org/abs/2209.11146).
16. Andrews, M. *et al.* DeepSNR: A deep learning foundation for offline gravitational wave detection. *arXiv e-prints* arXiv:2207.04749, DOI: [10.48550/arXiv.2207.04749](https://doi.org/10.48550/arXiv.2207.04749) (2022). [2207.04749](https://arxiv.org/abs/2207.04749).
17. Yu, H. & Adhikari, R. X. Nonlinear noise regression in gravitational-wave detectors with convolutional neural networks. *arXiv e-prints* arXiv:2111.03295, DOI: [10.48550/arXiv.2111.03295](https://doi.org/10.48550/arXiv.2111.03295) (2021). [2111.03295](https://arxiv.org/abs/2111.03295).
18. Moreno, E. A., Borzyszkowski, B., Pierini, M., Vlimant, J.-R. & Spiropulu, M. Source-agnostic gravitational-wave detection with recurrent autoencoders. *Mach. Learn. Sci. Tech.* **3**, 025001, DOI: [10.1088/2632-2153/ac5435](https://doi.org/10.1088/2632-2153/ac5435) (2022). [2107.12698](https://arxiv.org/abs/2107.12698).
19. Krastev, P. G. Real-Time Detection of Gravitational Waves from Binary Neutron Stars using Artificial Neural Networks. *Phys. Lett. B* **803**, 135330, DOI: [10.1016/j.physletb.2020.135330](https://doi.org/10.1016/j.physletb.2020.135330) (2020). [1908.03151](https://arxiv.org/abs/1908.03151).
20. Schäfer, M. B., Ohme, F. & Nitz, A. H. Detection of gravitational-wave signals from binary neutron star mergers using machine learning. *Phys. Rev. D* **102**, 063015, DOI: [10.1103/PhysRevD.102.063015](https://doi.org/10.1103/PhysRevD.102.063015) (2020). [2006.01509](https://arxiv.org/abs/2006.01509).
21. Miller, A. L. *et al.* How effective is machine learning to detect long transient gravitational waves from neutron stars in a real search? *Phys. Rev. D* **100**, 062005, DOI: [10.1103/PhysRevD.100.062005](https://doi.org/10.1103/PhysRevD.100.062005) (2019). [1909.02262](https://arxiv.org/abs/1909.02262).
22. Wei, W. & Huerta, E. A. Deep learning for gravitational wave forecasting of neutron star mergers. *Phys. Lett. B* **816**, 136185, DOI: [10.1016/j.physletb.2021.136185](https://doi.org/10.1016/j.physletb.2021.136185) (2021). [2010.09751](https://arxiv.org/abs/2010.09751).
23. Yu, H., Adhikari, R. X., Magee, R., Sachdev, S. & Chen, Y. Early warning of coalescing neutron-star and neutron-star-black-hole binaries from the nonstationary noise background using neural networks. *Phys. Rev. D* **104**, 062004, DOI: [10.1103/PhysRevD.104.062004](https://doi.org/10.1103/PhysRevD.104.062004) (2021). [2104.09438](https://arxiv.org/abs/2104.09438).
24. Qiu, R., Krastev, P., Gill, K. & Berger, E. Deep Learning Detection and Classification of Gravitational Waves from Neutron Star-Black Hole Mergers. *arXiv e-prints* arXiv:2210.15888, DOI: [10.48550/arXiv.2210.15888](https://doi.org/10.48550/arXiv.2210.15888) (2022). [2210.15888](https://arxiv.org/abs/2210.15888).
25. Wei, W. *et al.* Deep Learning with Quantized Neural Networks for Gravitational-wave Forecasting of Eccentric Compact Binary Coalescence. *The Astrophys. J.* **919**, 82, DOI: [10.3847/1538-4357/ac1121](https://doi.org/10.3847/1538-4357/ac1121) (2021). [2012.03963](https://arxiv.org/abs/2012.03963).
26. Cuoco, E. *et al.* Enhancing Gravitational-Wave Science with Machine Learning. *Mach. Learn. Sci. Tech.* **2**, 011002, DOI: [10.1088/2632-2153/abb93a](https://doi.org/10.1088/2632-2153/abb93a) (2021).
27. Huerta, E. A. & Zhao, Z. Advances in Machine and Deep Learning for Modeling and Real-Time Detection of Multi-messenger Sources. In *Handbook of Gravitational Wave Astronomy*, 47, DOI: [10.1007/978-981-15-4702-7_47-1](https://doi.org/10.1007/978-981-15-4702-7_47-1) (Springer, Singapore, 2021).
28. Huerta, E. A. *et al.* Enabling real-time multi-messenger astrophysics discoveries with deep learning. *Nat. Rev. Phys.* **1**, 600–608, DOI: [10.1038/s42254-019-0097-4](https://doi.org/10.1038/s42254-019-0097-4) (2019). [1911.11779](https://arxiv.org/abs/1911.11779).
29. Burgazli, A., Sergijenko, O. & Vavilova, I. Machine learning in cosmology and gravitational wave astronomy: recent trends. In *"Horizons in Computer Science Research"*, vol. 22, 193–240 (Nova Science Publisher Inc., 2022).
30. Huerta, E. A. *et al.* Convergence of Artificial Intelligence and High Performance Computing on NSF-supported Cyberinfrastructure. *J. Big Data* **7**, 88, DOI: [10.1186/s40537-020-00361-2](https://doi.org/10.1186/s40537-020-00361-2) (2020). [2003.08394](https://arxiv.org/abs/2003.08394).
31. Khan, A., Huerta, E. A. & Das, A. Physics-inspired deep learning to characterize the signal manifold of quasi-circular, spinning, non-precessing binary black hole mergers. *Phys. Lett. B* **808**, 135628, DOI: [10.1016/j.physletb.2020.135628](https://doi.org/10.1016/j.physletb.2020.135628) (2020). [2004.09524](https://arxiv.org/abs/2004.09524).
32. Khan, A., Huerta, E. A. & Kumar, P. AI and extreme scale computing to learn and infer the physics of higher order gravitational wave modes of quasi-circular, spinning, non-precessing black hole mergers. *Phys. Lett. B* **835**, 137505, DOI: [10.1016/j.physletb.2022.137505](https://doi.org/10.1016/j.physletb.2022.137505) (2022). [2112.07669](https://arxiv.org/abs/2112.07669).
33. Wei, W., Khan, A., Huerta, E. A., Huang, X. & Tian, M. Deep learning ensemble for real-time gravitational wave detection of spinning binary black hole mergers. *Phys. Lett. B* **812**, 136029, DOI: [10.1016/j.physletb.2020.136029](https://doi.org/10.1016/j.physletb.2020.136029) (2021). [2010.15845](https://arxiv.org/abs/2010.15845).
34. Huerta, E. A. *et al.* Accelerated, scalable and reproducible AI-driven gravitational wave detection. *Nat. Astron.* **5**, 1062–1068, DOI: [10.1038/s41550-021-01405-0](https://doi.org/10.1038/s41550-021-01405-0) (2021). [2012.08545](https://arxiv.org/abs/2012.08545).
35. Chaturvedi, P., Khan, A., Tian, M., Huerta, E. A. & Zheng, H. Inference-Optimized AI and High Performance Computing for Gravitational Wave Detection at Scale. *Front. Artif. Intell.* **5**, 828672, DOI: [10.3389/frai.2022.828672](https://doi.org/10.3389/frai.2022.828672) (2022). [2201.11133](https://arxiv.org/abs/2201.11133).

36. Pratten, G. *et al.* Computationally efficient models for the dominant and subdominant harmonic modes of precessing binary black holes. *Phys. Rev. D* **103**, 104056, DOI: [10.1103/PhysRevD.103.104056](https://doi.org/10.1103/PhysRevD.103.104056) (2021). [2004.06503](https://arxiv.org/abs/2004.06503).
37. Vallisneri, M., Kanner, J., Williams, R., Weinstein, A. & Stephens, B. The LIGO Open Science Center. *J. Phys. Conf. Ser.* **610**, 012021, DOI: [10.1088/1742-6596/610/1/012021](https://doi.org/10.1088/1742-6596/610/1/012021) (2015). [1410.4839](https://arxiv.org/abs/1410.4839).
38. Abbott, B. P. *et al.* Prospects for observing and localizing gravitational-wave transients with advanced ligo, advanced virgo and kagra. *Living Rev. Relativ.* **23**, 3, DOI: [10.1007/s41114-020-00026-9](https://doi.org/10.1007/s41114-020-00026-9) (2020).
39. van den Oord, A. *et al.* WaveNet: A Generative Model for Raw Audio. In *9th ISCA Speech Synthesis Workshop*, 125–125 (2016).
40. Bruna, J., Zaremba, W., Szlam, A. & LeCun, Y. Spectral networks and locally connected networks on graphs. *arXiv preprint arXiv:1312.6203* (2013).
41. Gilmer, J., Schoenholz, S. S., Riley, P. F., Vinyals, O. & Dahl, G. E. Neural message passing for quantum chemistry. In *International conference on machine learning*, 1263–1272 (PMLR, 2017).
42. Hamilton, W., Ying, Z. & Leskovec, J. Inductive representation learning on large graphs. In Guyon, I. *et al.* (eds.) *Advances in Neural Information Processing Systems*, vol. 30 (Curran Associates, Inc., 2017).
43. Velickovic, P. *et al.* Graph attention networks. *stat* **1050**, 10–48550 (2017).
44. Xu, K., Hu, W., Leskovec, J. & Jegelka, S. How powerful are graph neural networks? *arXiv preprint arXiv:1810.00826* (2018).

Acknowledgements

This work was supported by Laboratory Directed Research and Development (LDRD) funding from Argonne National Laboratory, provided by the Director, Office of Science, of the U.S. Department of Energy under Contract No. DE-AC02-06CH11357. It used resources of the Argonne Leadership Computing Facility, which is a DOE Office of Science User Facility supported under Contract DE-AC02-06CH11357. E.A.H. and M.T. gratefully acknowledge support from National Science Foundation award OAC-1931561. This research used resources of the Argonne Leadership Computing Facility, which is a DOE Office of Science User Facility supported under Contract DE-AC02-06CH11357. This research used the Delta advanced computing and data resource which is supported by the National Science Foundation (award OAC 2005572) and the State of Illinois. Delta is a joint effort of the University of Illinois at Urbana-Champaign and its National Center for Supercomputing Applications.

Author contributions statement

E.A.H. envisioned and led this work, and guided the design of AI models. M.T. designed novel approaches to develop the neural networks introduced in this article, and tested their performance with a variety of uncertainty quantification metrics. H.Z. distributed the training and inference of AI models in the Polaris supercomputer. All authors contributed to the writing of this manuscript.

Competing interests

The authors declare no competing financial and/or non-financial interests in relation to the work described in this manuscript.